

Aerosol Nanoencapsulation: Single-Pass Floating Self-Assembly of Biofunctional Hybrid Nanoplatfoms

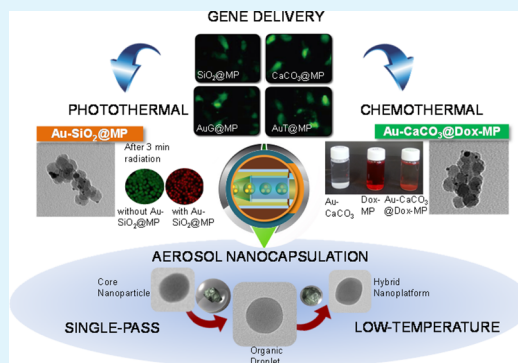
Jeong Hoon Byeon*

School of Mechanical Engineering, Yeungnam University, Gyeongsan 38541, Republic of Korea

S Supporting Information

ABSTRACT: Multifunctional nanoplatfoms were prepared via floating self-assembly using a hard nanoparticle (NP) as the core and a modified-polymer (MP, cholesterol-chitosan linked with polyethylenimine) droplet as the shell in a single-pass aerosol nanoencapsulation process. The floating hard NPs (silica, calcium carbonate, gold-decorated graphene oxide, and thiol-capped gold) were directly injected into MP droplets at the opening of a spraying device. Subsequently, the solvent was thermally extracted from the droplets, resulting in the formation of biofunctional nanoplatfoms. Measured in vitro, the genes complexed with the nanoplatfoms were transfected into target cells, exhibiting higher efficiencies for the MP particles alone without a significant increase in in vitro cell cytotoxicity. The aerosol encapsulation could be further extended to prepare other combinations [gold-silica and gold-calcium carbonate including doxorubicin (Dox)] using the MP, and their hybrid natures demonstrated photothermal cancer cell killing and chemo-thermal Dox release capabilities through surface plasmon resonance heating.

KEYWORDS: multifunctional nanoplatfoms, aerosol nanoencapsulation, gene delivery, photothermal killing, chemo-thermal release



Finely synthesized and modified nanoparticles (NPs) of size 20–500 nm are widely employed for therapeutic, diagnostic, and theranostic (i.e., both therapeutic and diagnostic) purposes. The large active surface areas of NPs can improve their ability to bind and deliver functional components such as drugs, proteins, and probe materials in order to efficiently treat and diagnose cells and tissues.^{1,2} On this account, numerous approaches to prepare/modify biofunctional NPs have been investigated for enhancement in biomedical applications. Even though many nanoplatfoms have been recently introduced for nanomedicine through the use of wet chemical methods,^{3,4} further study is still required to improve the properties and effectiveness of such platforms, including preparation strategies for their practical usage.

Researchers have favored chitosan as a biocompatible platform in recent years due to its favorable physicochemical properties and scalability. Thus, chitosan and its modified forms are widely employed as carriers, scaffolds, and protective/antibacterial layers in therapeutic applications.^{5,6} More recently, chitosan modifications were attempted by incorporating fatty acids, folates, cationic compounds,^{6–9} and so on to enhance the biochemical interaction and transfection into cells for more practical applications.¹⁰ In the area of therapeutics, modifications with lipids or polyethylenimines (PEI) have been frequently investigated and demonstrated to improve the biofunctionality without a significant increase in cytotoxicity/side effects.

Researchers have also become interested in incorporating or combining biofunctional organic/polymeric compounds with

other functional components in order to enhance or complement their properties.^{11,12} In particular, inorganic NPs-incorporated hybrid nanoplatfoms are extensively employed in biomedical applications for external stimuli-responsive controlled drug release and enhanced traceability.¹³ Specifically, in recent years, various metallic NPs have been incorporated with biofunctional organic components for photo- or chemo-thermal therapies due to surface plasmon resonance heating when they are placed in cells under infrared (IR) or near-infrared (NIR) irradiation.¹³

Although researchers have proposed many wet chemistry formulations based on the suspension of metallic particles for biomedical applications, such formulations may only be workable (and possess the desired performance) for a short period of time. In addition, organic or polymeric components incorporated with metallic NPs are normally unstable due to gradual degradation by hydrolysis; biofunctional nanomaterials in a suspension or colloidal form are therefore not recommended.¹⁴ Nanomaterials in a colloidal form also tend to aggregate during storage, thus changing the materials' properties and making them less suitable for bioapplications.¹⁵ As a result, we require a paradigm shift in our strategy for preparing stable organic–inorganic hybrid nanomaterials with a simpler and more versatile processing method for efficient use in biomedical applications.

Received: May 21, 2016

Accepted: July 6, 2016

Published: July 6, 2016



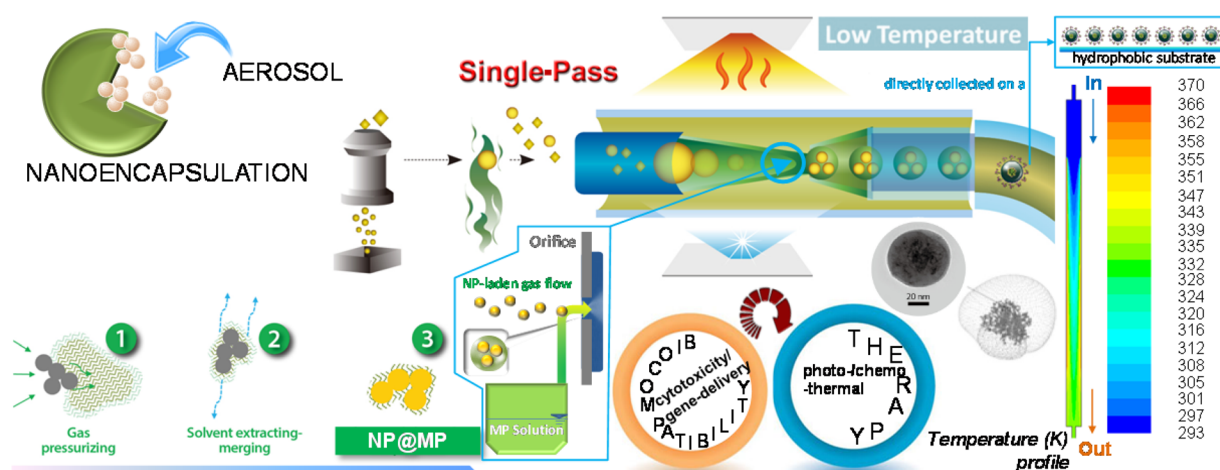


Figure 1. Schematic of aerosol nanoencapsulation for preparing NP@MP using a series connection of an aerosol NP generator and an MP encapsulator.

A single-pass aerosol route is an alternative method for preparing such nanomaterials with fewer preparation steps; such a process can allow long-term storage of the prepared nanomaterials in powdered form.¹⁶ Aerosol techniques in biomedical applications are generally employed for the treatment of bronchopulmonary disease via the delivery of therapeutic agents to the mucosa of the respiratory tract and pulmonary alveoli;¹⁷ more recently, researchers have further applied and/or modified these techniques to prepare micro- or nanoscale biofunctional hybrid materials for other therapeutic applications.^{18,19} However, because the conventional aerosol route of most materials is commonly performed under high-temperature conditions (500 °C and above), this process can only be used for fabricating inorganic-based materials.²⁰ When using a single-pass aerosol route for the production of the inorganic part of hybrid materials, it is essential to perform further treatments (i.e., incorporation with organic or polymeric compounds) before the materials will be suitable for use.¹⁶ It is thus necessary to use low-temperature processing, as temperatures above 300 °C will decompose most organic or polymeric materials (i.e., biofunctional soft materials).²¹

This study introduces a single-pass, low-temperature aerosol nanoencapsulation method for preparing multibiofunctional nanoplateforms consisting of a hard NP (silica, SiO₂; calcium carbonate, CaCO₃; Au-decorated graphene oxide, AuG; or thiol-capped Au, AuT) as the core and a modified-polymer (MP; cholesterol-chitosan linked with PEI) as the shell. To enhance the delivery of drugs, genes, vaccines, and tracing agents into target cells, polymer-incorporated SiO₂,²² CaCO₃,²³ Au,²⁴ graphene,²⁵ and thiol²⁶ nanoplateforms have been employed. In one recent study, MP was chosen, because it has an enhanced cationic charge with low toxicity and high affinity to hard NPs¹² and has been aerosolized to enhance the performance of gene delivery into mammalian cells without using multiple wet chemical processes.²⁷ Despite the successful use of both components, the preparation systems of hybrid nanoplateforms should be modified and reconstructed when the compartment replacement of the platforms is required to produce a different function.²² Consequently, the introduction of practical generalizable assembly strategies in a built-to-order configuration is a huge challenge in the preparation of various desired nanoplateforms without significant changes to the preparation system. To perform nanoencapsulation (Figure

1), we directly injected floating hard NPs into MP droplets using a spray device and subsequently heat-treated them (<90 °C wall temperature) to liberate the solvent from the droplets, resulting in the formation of multibiofunctional nanoplateforms. The assembled nanoplateforms were electrostatically collected on hydrophobic substrates to evaluate their ability in gene delivery and photo- (HeLa cell killing) and chemo-thermal [doxorubicin (Dox, Sigma-Aldrich, USA) release] activities after testing the cytotoxicity.

The particle size distribution in the aerosol state was analyzed using a scanning mobility particle sizer (model 3936, TSI, Shoreview, MN, USA) to verify the mean diameter, standard deviation (SD), and number concentration (Figure 2).

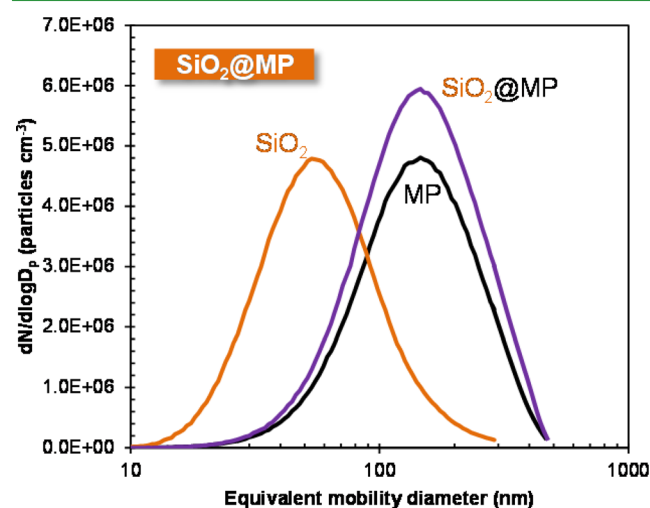


Figure 2. Size distributions of aerosol MP alone, individual NPs (SiO₂), and MP encapsulated NPs (SiO₂@MP).

The measured diameter, SD, and concentration of the SiO₂@MP hybrid structures were 130 nm, 1.85, and $3.4 \times 10^6 \text{ cm}^{-3}$, respectively (see Table S1). Data for SiO₂ NPs were 57 nm, 1.75, and $2.8 \times 10^6 \text{ cm}^{-3}$, respectively, and those for individual MP particles were 130 nm, 1.86, and $2.7 \times 10^6 \text{ cm}^{-3}$, respectively. The results showed only a new unimode size distribution; the distributions were closer among the MP particles than among the SiO₂ particles, which suggest that the SiO₂ particles were nearly quantitatively combined with the MP

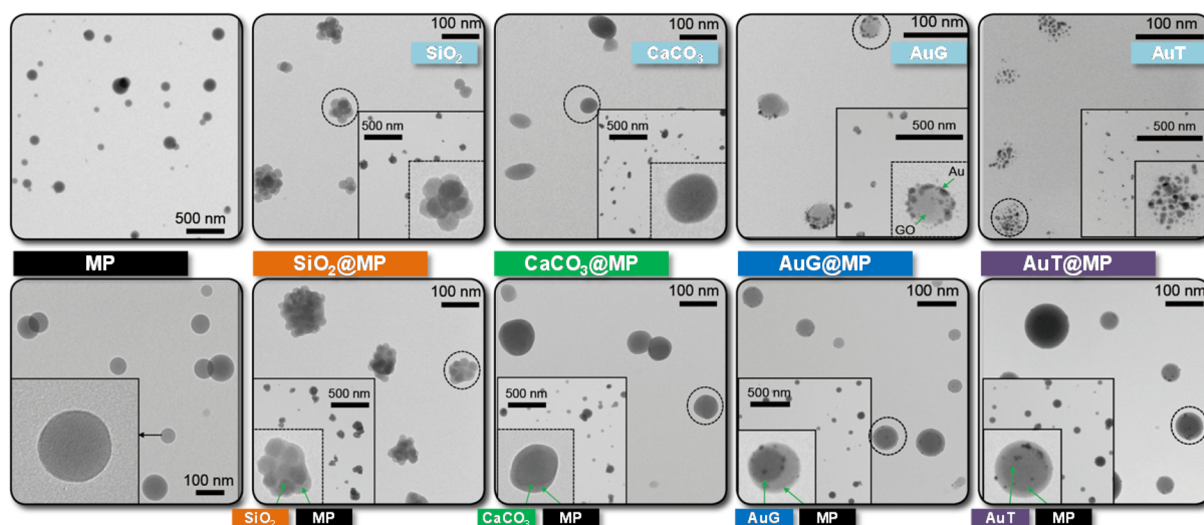


Figure 3. TEM images of MP alone (left), individual NPs (SiO₂, CaCO₃, AuG, or AuT) (top), and MP encapsulated NPs (SiO₂@, CaCO₃@, AuG@, or AuT@MP) (bottom).

components, forming MP-encapsulated SiO₂ NPs (i.e., SiO₂@MP nanoplateforms). Other cases (CaCO₃@MP, AuG@MP, and AuT@MP; Figure S1) also demonstrated this incorporation behavior. For an appropriate comparison, the diameter, SD, and concentration of aerosol NPs (SiO₂, CaCO₃, AuG, and AuT) were set to ~60 nm, ~1.75, and ~2.9 × 10⁶ cm⁻³, respectively.

Transmission electron microscope (TEM, CM-100, FEI/Philips, USA) images (Figure 3) indicate that the SiO₂ particles are agglomerate (consisting of individual SiO₂ nanocrystals), while the MP particles exhibit a similar spherical shape with a smooth surface and are separate from each other. Solid MP particles were obtained using this method, which was caused by the given drying rate and can be explained with the Peclet number, *Pe*, dimensionless number that represents the relative time-scales for diffusion (*D_d*²/4δ_v) and convective drying τ_d:

$$Pe = \frac{D_d^2}{4\tau_d\delta_v} \quad (1)$$

The *Pe* value of the current condition was significantly smaller than 1, indicating the migration of solutes at the interface toward the core region of droplets. It was sufficient to keep up with convective drying, thereby inducing the formation of dense solid particles. When the SiO₂ NPs passed through the opening of the atomizer (Figure 1), the SiO₂ particles were capsulated by the MP particles due to the gas pressure. In the heated tubular flow reactor, the gas temperature (Figure 1) was partially lower than the glass transition temperature of chitosan (140–150 °C). Consequently, the particles were not softened and a spherical morphology was maintained (i.e., the mechanical strength was sustained).²⁸ The high resolution TEM image shows a gray network shell around the SiO₂ core particles, implying the presence of an MP moiety that completely covered the SiO₂ particles. For CaCO₃@MP, MP encapsulated one CaCO₃ particle; thus, the morphology was more spherical compared with that of SiO₂@MP. AuG and AuT NPs were also capsulated by spherical MPs, but some particles protruded from the MP shell, probably because of their higher diffusivity to the MP shell. The diffusion coefficient *D* of a particle in a droplet is related to its size *D_p*,

$$D = \frac{kT}{3\pi\mu D_p} \quad (2)$$

where *k* is the Boltzmann constant, *T* is the temperature, and *μ* is the droplet viscosity. The diffusivity of the Au-based particles was approximately 15 times larger than that of the SiO₂ and CaCO₃ particles, and this induced the protrusion of Au particles from the MP shells. The efficiencies of MP encapsulation of SiO₂, CaCO₃, AuG, and AuT NPs were 96.4, 98.7, 91.9, and 90.1%, respectively, and were calculated using the following equation

$$\eta_{\text{encap}} = \left(1 - \frac{N}{N_0}\right)100(\%) \quad (3)$$

where *N*₀ and *N* are the number concentrations of NPs before and after encapsulation, respectively. The mean mode diameter of the MP particles was 125 ± 9.3 nm. The same data for the SiO₂@, CaCO₃@, AuG@, and AuT@MP nanocomposites were 131 ± 8.3, 128 ± 6.9, 138 ± 9.9, and 134 ± 8.1 nm, respectively, and these data are well matched with the data described in Figure 2 and Figure S1.

As shown in Figure S2, the IR spectrum (absorbance mode) (Nicolet 6700, Thermo Electron, Madison, WI, USA) of the MP particles showed bands at around 1664, 1580, and 1380 cm⁻¹, corresponding to amides I, II, and III, respectively. Other bands at 1160 and 1033 cm⁻¹ could be assigned to the asymmetric stretching of the C–O–C bridge and C–O, respectively; these peaks were attributed to the saccharine structure of chitosan. The MP further introduced two more broad bands at around 2950 and 3400 cm⁻¹, which were attributable to alkyl bends and amine-hydroxyl stretching vibrations, respectively. After the NP was capsulated by the MP, there were no significant differences between the MP and NP@MP, whereas the specific peak of the amide groups (II) intensified, especially for the SiO₂@, AuG@, and AuT@MP cases. This means that the NP may generate an effective linkage with amide groups. Furthermore, for the AuG@MP and AuT@MP cases, other amide groups (I and III) were intensively linked onto the NPs. In short, the changed spectra in the NP@MP platforms may indicate a DNA-binding ability to form NP@MP-gene complexes via electrostatic attraction. The zeta potential of NP@MP-gene complexes is described in Table S2.

The positive charges of the complexes suggest that the nanoplateforms may have potential for delivering genes into cells. The zeta potential varies with different NP@MP platforms; AuT and SiO₂ have the highest and lowest values, respectively, and these correspond with the peak characteristics of the IR spectra, although there were no significant differences in the zeta potential between the platforms.

An electrophoretic mobility shift experiment (not shown) was performed to confirm the formation of the nanoplateform-gene complexes for employing such complexes in a gene delivery test. To investigate the appropriate ranges of mass ratio (NP@MP platform to gene), we tested ratios of 0.2, 1.0, 5.0, 10.0, 20.0, and 50.0 to confirm the complexing efficiency. The 10.0 ratio was eventually chosen for the gene delivery tests, because nearly all the genes were efficiently bound with NP@MP platforms and clearly showed little gene liberation from the complexes.

The cytotoxicities of the platforms were then assessed, because one essential feature of any biomedical application of NP@MP platforms is that they must be biocompatible. Measurements of cell viability of the platforms were performed at different mass concentrations (5–100 $\mu\text{g mL}^{-1}$) using a 3-(4,5-dimethylthiazol-2-yl)-5-(3-carboxymethoxyphenyl)-2-(4-sulfophenyl)-2H-tetrazolium assay in 293 human embryonic kidney cells in comparison with cell viability only from the MP (Figure S3). The results show that cell viabilities were higher than 92.3% for all the tested NP@MP platforms, whereas a slightly better viability (>96.5%) was observed for the MP alone. This suggests that the incorporation of NPs did not increase the cytotoxicity of the MP particles, thereby providing evidence that there was no significant interference in the cells' reproductive abilities after incubation with the platforms. The slight cytotoxicity may be caused by cationic polymers, which may interfere with the critical intracellular processes of cells. The slightly higher cytotoxicities of the platforms at higher mass concentrations may be caused by damage via interactions between NP surfaces and cellular compartments. Specifically, enzymatic degradations and/or single-strand breaks of genes in cells via catalytic oxidative stress from NPs may have slightly increased the cytotoxicities at higher mass concentrations.²⁹

The gene delivery performance of the platforms was then evaluated using luminescence measurements of green fluorescent protein (GFP) genes. The results [shown in Figure 4a, expressed as relative luminescent units (RLUs) mg^{-1} of protein] from the platforms complexed with the GFP genes were compared with the results from the MP particle-GFP gene complexes. As a control, the gene delivery performance of naked DNA was first attempted for comparison purposes; the intensity of GFP fluorescence reached approximately 1.1×10^4 RLU mg^{-1} in the 293 cells. The results were significantly enhanced (i.e., intracellular transfection was achieved) when employing MP (1.33×10^6 RLU mg^{-1}) and platforms (1.7×10^6 to 2.6×10^6 RLU mg^{-1}); all platforms showed higher delivery performances. As shown in Figure 4b, the corresponding fluorescent microscope images further confirmed the different gene delivery abilities of the complexes. According to the zeta potential data (20–27 mV, Table S2), the differences in gene delivery may have been caused by different bindings between an NP and MP, providing different levels of gene delivery (1.3×10^6 to 2.6×10^6 RLU mg^{-1}) since there is no significant difference in particle size between the nanoplateforms. The AuT@MP platforms demonstrated the highest efficiency because AuT can more easily bind with functionaliz-

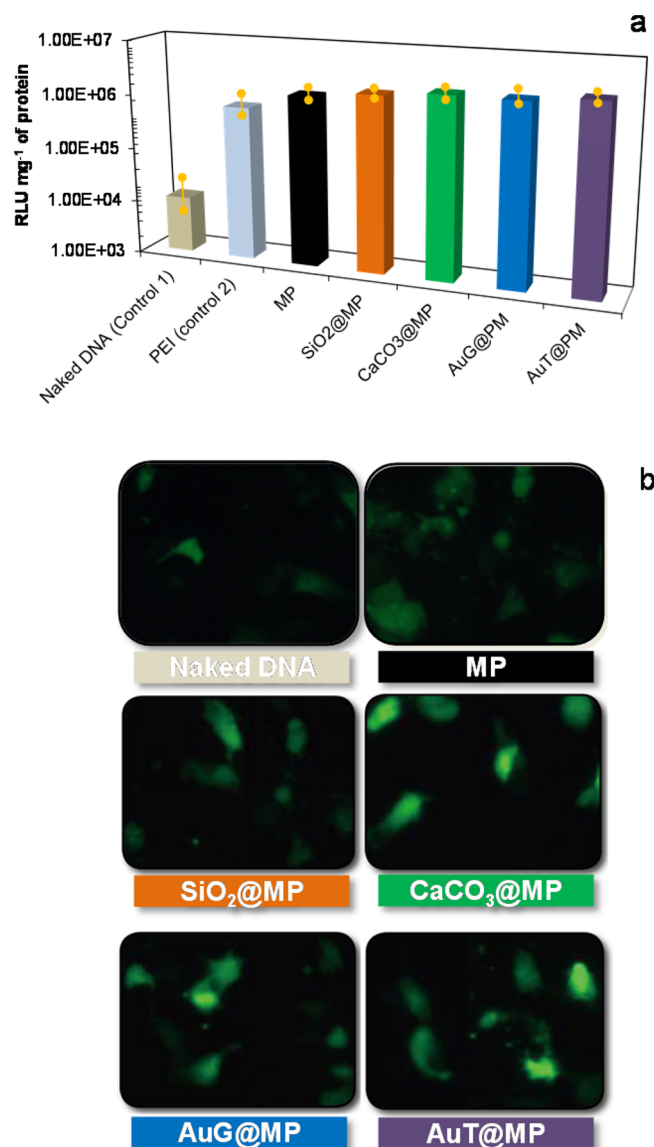


Figure 4. (a) Gene delivery performances and (b) fluorescent expressions of MP alone, and NP@MP nanoplateforms (SiO₂@, CaCO₃@, AuG@, or AuT@MP) in 293 human embryonic kidney cells over 24 h.

ing or targeting ligands (i.e., inducing a high affinity between the luciferase and thiol groups in complexes) than other materials;³⁰ additionally, its protruded characteristics from the MP shell enhanced the interaction with cell surface receptors and thus may affect the amount of gene transfection.

To evaluate the multifunctional ability of nanoplateforms produced using the proposed processing method, we further prepared and employed Au-SiO₂@MP (left TEM image) and Au-CaCO₃@Dox-MP (right TEM image) platforms as nanoplateforms for applications in photothermal therapy and the chemo-thermal release of Dox, respectively. The left side of Figure 5 shows the change in temperature (measured using an IR thermometer) of phosphate-buffered saline (PBS, Sigma-Aldrich, USA) containing Au-SiO₂@MP platforms. The temperature increase (2.3–14.9 $^{\circ}\text{C}$) is proportional to the mass concentration (5–100 $\mu\text{g mL}^{-1}$). From the temperature measurements, it can be concluded that the Au-SiO₂@MP platforms absorbed the irradiated laser light, and the light was

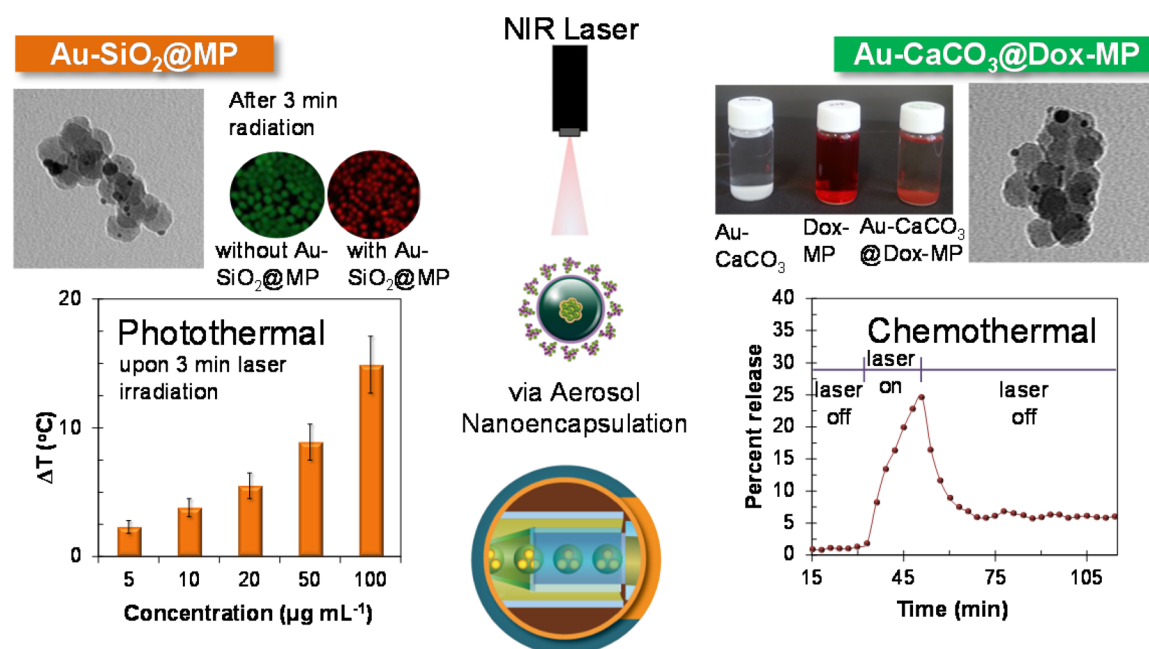


Figure 5. Results of photothermal therapy using Au-SiO₂@MP (left TEM image) and chemo-thermal Dox release from Au-CaCO₃@Dox-MP (right TEM image) under laser irradiation with a 705 nm wavelength. Temperature increases (left) for different mass concentrations (from 5 to 100 $\mu\text{g mL}^{-1}$) under 705 nm laser irradiation for a duration of 3 min (1.8 W cm^{-2}). Representative fluorescence images of HeLa cells without (green, viable) and with (red, dead) Au-SiO₂@MP under laser irradiation. NIR-induced release of Dox (right) from Au-CaCO₃@Dox-MP. A photograph (right) shows Au-CaCO₃, Dox-MP, and Au-CaCO₃@Dox-MP samples in PBS solution.

successively converted into thermal energy. On the basis of this conversion upon 705 nm excitation, *in vitro* photothermal therapy using the NPs was investigated. Viable or dead cells were differentiated using calcein AM (viable cells, green fluorescence, Life Technologies, USA) and propidium iodide (dead cells, red fluorescence, Life Technologies, USA) after laser irradiation. In the control group (laser irradiation in the absence of Au-SiO₂@MP), all cells displayed green fluorescence, thus showing that the irradiation had no significant cytotoxic effects. When the platforms were exposed to laser irradiation for 3 min, the platforms exhibited a photothermal effect for HeLa cells; hence, nearly all cells that were placed inside the circle of the laser spot were killed and exhibited homogeneous red fluorescence. The cells incubated without the platforms mostly stayed alive, exhibiting green fluorescence. The right side of Figure 5 shows the Dox release behavior from Au-CaCO₃@Dox-MP platforms. The platforms sampled using a hydrophobic substrate were injected into a PBS solution and exposed to the laser. The irradiation enhanced the Dox release from the platforms, and the release pattern (i.e., a drastic increase in the Dox release with the temperature) coincided with the temperature increase pattern. The converted heat upon irradiation enhances Dox release from the NPs since heat may promote the oscillation of Dox molecules adsorbed by the platforms. As can be seen in the photographs (the right side of Figure 5), the reddish color of Dox-MP turned pale after it was combined with Au-CaCO₃, implying that most of the Dox was adsorbed in Au-CaCO₃ (particularly in CaCO₃), and that its release can be triggered by laser irradiation. From the photoderived activities, the proposed processing method may enable the fabrication of various multifunctional nanoplateforms for use in biomedical applications.

A single-pass aerosol nanoencapsulation method for preparing MP-encapsulated NP platforms has been employed in gene delivery, photothermal therapy, and chemo-thermal

release after testing the biocompatibility. It exhibited a slightly higher cytotoxicity but better gene delivery efficiencies in 293 human embryonic kidney cells when compared to the MP alone. Other nanoplateforms (Au-SiO₂@MP and Au-CaCO₃@Dox-MP) produced using the proposed processing method were further available for photothermal cancer cell killing and chemo-thermal Dox release activities without the use of additional chemical processes. This new strategy can thus enable the on-demand continuous fabrication and modification of fresh multibiofunctional nanoplateforms for use in various biomedical applications, which may further generalize to a wide range of theranostic applications, and may also hold immense promise for biomaterial coatings.

■ ASSOCIATED CONTENT

§ Supporting Information

The Supporting Information is available free of charge on the ACS Publications website at DOI: 10.1021/acsami.6b06085.

Experimental details, particle size distributions of other platform configurations, FTIR spectra and cytotoxicities of platforms, and summaries of size distribution and zeta potential of platforms (PDF)

■ AUTHOR INFORMATION

Corresponding Author

*E-mail: postjb@yu.ac.kr. Tel. +82-53-810-2451.

Notes

The author declares no competing financial interest.

■ ACKNOWLEDGMENTS

This work was supported by the National Research Foundation of Korea Grant funded by the Korean Government (NRF-2015R1A2A2A04005809).

REFERENCES

- (1) Nel, A. E.; Madler, L.; Velegol, D.; Xia, T.; Hoek, E. M. V.; Somasundaran, P.; Klaessig, F.; Castranova, V.; Thompson, M. Understanding Biophysicochemical Interactions at the Nano-Bio Interface. *Nat. Mater.* **2009**, *8*, 543–557.
- (2) Karmi, A.; Hussein, G. A.; Faroun, M.; Sowwan, M. Multifunctional Nanovehicles for Combined 5-Fluorouracil and Gold Nanoparticles Based on the Nanoprecipitation Method. *J. Nanosci. Nanotechnol.* **2011**, *11*, 4675–4683.
- (3) De, M.; Ghosh, P. S.; Rotello, V. M. Applications of Nanoparticles in Biology. *Adv. Mater.* **2008**, *20*, 4225–4241.
- (4) Murphy, C. J.; Gole, A. M.; Stone, J. W.; Sisco, P. N.; Alkilany, A. M.; Goldsmith, E. C.; Baxter, S. C. Gold Nanoparticles in Biology: Beyond Toxicity to Cellular Imaging. *Acc. Chem. Res.* **2008**, *41*, 1721–1730.
- (5) Ducepe, N.; Tabrizian, M. Advances in Using Chitosan-Based Nanoparticles for In Vitro and In Vivo Drug and Gene Delivery. *Expert Opin. Drug Delivery* **2010**, *7*, 1191–1207.
- (6) Liang, X. F.; Wang, H. J.; Luo, H.; Tian, H.; Zhang, B. B.; Hao, L. J.; Teng, J. I.; Chang, J. Characterization of Novel Multifunctional Cationic Polymeric Liposomes Formed from Octadecyl Quaternized Carboxymethyl Chitosan/Cholesterol and Drug Encapsulation. *Langmuir* **2008**, *24*, 7147–7153.
- (7) Yang, S. J.; Lin, F. H.; Tsai, K. C.; Wei, M. F.; Tsai, H. M.; Wong, J. M.; Shieh, M. J. Folic Acid-Conjugated Chitosan Nanoparticles Enhanced Porphyrin IX Accumulation in Colorectal Cancer Cells. *Bioconjugate Chem.* **2010**, *21*, 679–689.
- (8) Kievit, F. M.; Veis, O.; Bhattacharjee, N.; Fang, C.; Gunn, J. W.; Lee, D.; Ellenbogen, R. G.; Olson, J. M.; Zhang, M. Q. PEI-PEG-Chitosan Copolymer Coated Iron Oxide Nanoparticles for Safe Gene Delivery: Synthesis, Complexation, and Transfection. *Adv. Funct. Mater.* **2009**, *19*, 2244–2251.
- (9) Yu, H.; Deng, C.; Tian, H.; Lu, T.; Chen, X.; Jing, X. Chemo-Physical and Biological Evaluation of Poly(L-lysine)-Grafted Chitosan Copolymers Used for Highly Efficient Gene Delivery. *Macromol. Biosci.* **2011**, *11*, 352–361.
- (10) Nandanan, E.; Jana, N. R.; Ying, J. Y. Functionalization of Gold Nanospheres and Nanorods by Chitosan Oligosaccharide Derivatives. *Adv. Mater.* **2008**, *20*, 2068–2073.
- (11) Tan, W. B.; Zhang, Y. Study of Chitosan Coatings on Nanoparticles for Biomedical Applications. *Int. J. Nanosci.* **2004**, *3*, 685–689.
- (12) Maity, A. R.; Jana, N. R. Chitosan-Cholesterol-Based Cellular Delivery of Anionic Nanoparticles. *J. Phys. Chem. C* **2011**, *115*, 137–144.
- (13) Huang, Y.; Xiao, Q.; Hu, H.; Zhang, K.; Feng, Y.; Li, F.; Wang, J.; Ding, X.; Jiang, J.; Li, Y.; Shi, L.; Lin, H. 915 nm Light-Triggered Photodynamic Therapy and MR/CT Dual-Modal Imaging of Tumor Based on the Nonstoichiometric $\text{Na}_{0.52}\text{YbF}_{3.52}:\text{Er}$ Upconversion Nanoprobes. *Small* **2016**, DOI: 10.1002/sml.201601023.
- (14) Bulmus, V.; Chan, Y.; Nguyen, Q.; Tran, H. L. Synthesis and Characterization of Degradable p(HEMA) Microgels: Use of Acid-Labile Crosslinkers. *Macromol. Biosci.* **2007**, *7*, 446–455.
- (15) Flores-Fernández, G. M.; Solá, R. J.; Griebenow, K. The Relation Between Moisture-Induced Aggregation and Structural Changes in Lyophilized Insulin. *J. Pharm. Pharmacol.* **2009**, *61*, 1555–1561.
- (16) Boissière, C.; Grosso, D.; Chaumonnot, A.; Nicole, L.; Sanchez, C. Aerosol Route to Functional Nanostructured Inorganic and Hybrid Porous Materials. *Adv. Mater.* **2011**, *23*, 599–623.
- (17) Edwards, D. A.; Dunbar, C. Bioengineering of Therapeutic Aerosols. *Annu. Rev. Biomed. Eng.* **2002**, *4*, 93–107.
- (18) Colilla, M.; Manzano, M.; Izquierdo-Barba, I.; Vallet-Regí, M.; Boissière, C.; Sanchez, C. Advanced Drug Delivery Vectors with Tailored Surface Properties Made of Mesoporous Binary Oxides Submicronic Spheres. *Chem. Mater.* **2010**, *22*, 1821–1830.
- (19) Liu, J.; Jiang, X.; Ashley, C.; Brinker, C. J. Electrostatically Mediated Liposome Fusion and Lipid Exchange with a Nanoparticle-Supported Bilayer for Control of Surface Charge, Drug Containment, and Delivery. *J. Am. Chem. Soc.* **2009**, *131*, 7567–7569.
- (20) Iskandar, F.; Mikrajuddin; Okuyama, K. Controllability of Pore Size and Porosity on Self-Organized Porous Silica Particles. *Nano Lett.* **2002**, *2*, 389–392.
- (21) Sanchez, C.; Soler-illia, G. J. d. A. A.; Ribot, F.; Lalot, T.; Mayer, C. R.; Cabuil, V. Designed Hybrid Organic–Inorganic Nanocomposites from Functional Nanobuilding Blocks. *Chem. Mater.* **2001**, *13*, 3061–3083.
- (22) Tang, H.; Guo, J.; Sun, Y.; Chang, B.; Ren, Q.; Yang, W. Facile Synthesis of pH Sensitive Polymer-Coated Mesoporous Silica Nanoparticles and Their Application in Drug Delivery. *Int. J. Pharm.* **2011**, *421*, 388–396.
- (23) Powell, T. J.; Palath, N.; DeRome, M. E.; Tang, J.; Jacobs, A.; Boyd, J. G. Synthetic Nanoparticle Vaccines Produced by Layer-by-Layer Assembly of Artificial Biofilms Induce Potent Protective T-Cell and Antibody Responses In Vivo. *Vaccine* **2011**, *29*, 558–569.
- (24) Byeon, J. H.; Kim, Y.-W. Gas-Phase Self-Assembly of Soft Nanocomposites for Efficient Gene Transfection and Photothermal Therapy. *J. Mater. Chem. B* **2014**, *2*, 3185–3189.
- (25) Bao, H.; Pan, Y.; Ping, Y.; Sahoo, N. G.; Wu, T.; Li, L.; Li, J.; Gan, L. H. Chitosan-Functionalized Graphene Oxide as a Nanocarrier for Drug and Gene Delivery. *Small* **2011**, *7*, 1569–1578.
- (26) Ding, Y.; Gu, G.; Xia, X.-H.; Huo, Q. Cysteine-Grafted Chitosan-Mediated Gold Nanoparticle Assembly: From Nanochains to Microcubes. *J. Mater. Chem.* **2009**, *19*, 795–799.
- (27) Byeon, J. H.; Kim, H.-K.; Thompson, D. H.; Roberts, J. T. Aerosol-Based Fabrication of Modified Chitosans and Their Application for Gene Transfection. *ACS Appl. Mater. Interfaces* **2014**, *6*, 4597–4602.
- (28) Dong, Y.; Ruan, Y.; Wang, H.; Zhao, Y.; Bi, D. Studies on Glass Transition Temperature of Chitosan with Four Techniques. *J. Appl. Polym. Sci.* **2004**, *93*, 1553–1558.
- (29) Guildford, A. L.; Poletti, T.; Osbourne, L. H.; Di Cerbo, A.; Gatti, A. M.; Santin, M. Nanoparticles of a Different Source Induce Different Patterns of Activation in Key Biochemical and Cellular Components of the Host Response. *J. R. Soc., Interface* **2009**, *6*, 1213–1221.
- (30) Lewinski, N.; Colvin, V.; Drezek, R. Cytotoxicity of Nanoparticles. *Small* **2008**, *4*, 26–49.